Computer Methods in Biomechanics and Biomedical Engineering

Publication details, including instructions for authors and subscription information:
http://www.tandfonline.com/loi/gcmb20

Finite element study of a tissue-engineered cartilage transplant in human tibiofemoral joint

Ali Vahdati [a] & Diane R. Wagner [a]

[a] Bioengineering Graduate Program, Aerospace and Mechanical Engineering Department, University of Notre Dame, Notre Dame, IN, USA

Available online: 02 Aug 2011

To cite this article: Ali Vahdati & Diane R. Wagner (2011): Finite element study of a tissue-engineered cartilage transplant in human tibiofemoral joint, Computer Methods in Biomechanics and Biomedical Engineering, DOI:10.1080/10255842.2011.585974

To link to this article: http://dx.doi.org/10.1080/10255842.2011.585974

Computer Methods in Biomechanics and Biomedical Engineering
iFirst article, 2011, 1–11

Taylor & Francis
Taylor & Francis Group

Finite element study of a tissue-engineered cartilage transplant in human tibiofemoral joint

Ali Vahdati and Diane R. Wagner*

Bioengineering Graduate Program, Aerospace and Mechanical Engineering Department, University of Notre Dame, Notre Dame, IN, USA

(*Received 23 September 2010; final version received 3 May 2011*)

Most tissue-engineered cartilage constructs are more compliant than native articular cartilage (AC) and are poorly integrated to the surrounding tissue. To investigate the effect of an implanted tissue-engineered construct (TEC) with these inferior properties on the mechanical environment of both the engineered and adjacent native tissues, a finite element study was conducted. Biphasic swelling was used to model tibial cartilage and an implanted TEC with the material properties of either native tissue or a decreased elastic modulus and fixed charged density. Creep loading was applied with a rigid impermeable indenter that represented the femur. In comparison with an intact joint, compressive strains in the transplant, surface contact stress in the adjacent native AC and load partitioning between different phases of cartilage were affected by inferior properties of TEC. Results of this study may lead to a better understanding of the complex mechanical environment of an implanted TEC.

Keywords: chondral defect; articular cartilage repair; osteochondral tissue engineering; finite element method; biphasic swelling

1. Introduction

Chondral and osteochondral defects of the knee occur due to a variety of reasons such as trauma, osteochondritis dissecans and joint instability (Sellards et al. 2002) and affect approximately 900,000 individuals in USA alone each year (Minas and Nehrer 1997). In addition to activity-specific pain associated with these lesions, they can lead to osteoarthritis if they remain untreated (Cicuttini et al. 2005; Ding et al. 2005). Current treatment methods including autologous chondrocyte implantation, osteochondral allograft or autograft transplantation and microfracture suffer from limitations such as the amount of material available, insufficient formation of hyaline cartilage, donor site morbidity, lack of durability and inability to integrate at the cartilage interface (Lattermann et al. 2006; Richter 2007; McNickle et al. 2008). Recently, tissue engineering has emerged as a potential treatment method and significant effort has been invested in developing chondral and osteochondral tissue-engineered constructs (TECs).

In spite of some success in engineering cartilaginous tissue, most TECs show inferior biomechanical and biochemical properties compared with native articular cartilage (AC; Hunziker 2002; Babalola and Bonassar 2009; Zhang et al. 2009; Huang et al. 2010). Inferior properties of TECs could alter the complex biomechanical environment of the knee joint, modulating the stress and strain fields experienced by both the implanted and native cells. The modified mechanical environment may directly damage the cells or provide signals via mechanotransduction that guide cells away from cartilage matrix production. Another challenge in engineering cartilage repair is the integration of the repair tissue with the adjacent native cartilage. If the implant is not firmly fixed to the surrounding native tissue, integration may be made more difficult by separation between the two tissues at the interface, or relative motion between them. In addition, lack of integration may further alter the mechanical environment, hinder cartilage regeneration at the defect site and lead to implant failure.

Computer simulations are a powerful tool to predict the mechanical environment of implanted TEC. Several authors have previously performed finite element (FE) simulations of repair or tissue-engineered cartilage in the knee joint. Wayne et al. (1991a, 1991b) used a $u-p$ FE numerical procedure to examine *in-vivo* behaviour of repair cartilage in a full-thickness chondral defect. Using axisymmetric FE models, Wu et al. (2002) studied the effect of press fit tolerance and the placement of an osteochondral plug on knee joint contact mechanics. Owen and Wayne (2006, 2011) performed an FE study on the effect of the superficial tangential zone on biomechanical performance of a transplanted chondral TEC. Using an FE model of the human knee, Pena et al. (2007) examined the effect of size and location of a full-thickness chondral defect on strain and stress distributions in repair tissue and around the defect rim both before and after partial healing. More recently, Mononen et al. (2010) looked at the effect

*Corresponding author. Email: dwagner@nd.edu

ISSN 1025-5842 print/ISSN 1476-8259 online

DOI: 10.1080/10255842.2011.585974
http://www.informaworld.com

of collagen fibril network structure and properties on mechanical behaviour of osteoarthritic and repair cartilage. Several authors have investigated the repair and remodelling process in chondral and osteochondral defects using mechanoregulation algorithms and indentation simulations (Hale et al. 1993; Smith and Mansour 2000; Duda et al. 2005; Kelly and Prendergast 2006).

However, none of the previous studies addressed the mechanical environment of a TEC with inferior properties and lack of integration at the implantation site. Our objectives here were to create an FE model of TEC transplanted in a focal cartilage defect in the knee joint and to investigate the effects of a lower modulus, lower proteoglycan (PG) content and a lack of integration at the interface on the mechanical environment of the implanted TEC and the surrounding native tissue. We also report the mechanical factors that may influence the integrative cartilage repair process at the engineered/native tissue interface.

2. Methods

2.1 Constitutive model

Using commercial FE package ABAQUS® (version 6.8-2, SIMULIA, Inc., Providence, RI, USA), we generated two-dimensional (2D) axisymmetric models of the medial compartment of a human tibiofemoral joint. The femur was modelled as a rigid impermeable indenter, whereas the fluid and solid phases and fixed charge densities (FCDs) in tibial AC were represented with a biphasic swelling model (Wilson et al. 2005a). Biphasic swelling is computationally less expensive than triphasic (Lai et al. 1991) and quadriphasic (Huyghe 1997; van Loon et al. 2003) models and thus is advantageous for geometrically large problems. Biphasic swelling and quadriphasic models show good agreement with one another in confined compression, 1D swelling and 2D simulations (Wilson et al. 2005a). In brief, the biphasic swelling model defines the total stress in the tissue as

$$\boldsymbol{\sigma} = -p\mathbf{I} + (\boldsymbol{\sigma}_\mathbf{s} - (\Delta\Pi)\mathbf{I}), \tag{1}$$

in which p is fluid hydrostatic pressure, $\Delta\Pi$ is the osmotic pressure difference, $\boldsymbol{\sigma}_\mathbf{s}$ is the solid matrix stress and $\mathbf{I}$ is the unit tensor (Wilson et al. 2005a, 2005b).

The osmotic swelling pressure gradient is calculated as

$$\Delta\Pi = \Phi_{\text{in}} RT\sqrt{(c_\text{F}^2 + 4c_{\text{ext}}^2)} - \Phi_{\text{ext}} RT, \tag{2}$$

in which Φ_{in} is the internal osmotic coefficient, Φ_{ext} is the external osmotic coefficient and R is the gas constant (Wilson et al. 2005a). In biphasic swelling, it is assumed that the external salt concentration c_{ext} and temperature T remain constant, thus the FCD c_F is the only variable in this equation and is deformation dependent as follows:

$$c_\text{F} = c_{\text{F0}} \frac{n_{\text{f0}}}{(n_{\text{f0}} - 1 + J)}, \tag{3}$$

in which c_{F0} is initial FCD, J is the determinant of the deformation gradient tensor $\mathbf{F}$ and n_{f0} is the initial fluid fraction (Wilson et al. 2005a).

Constitutive behaviour of the solid matrix is represented by a compressible Neo-Hookean model:

$$\boldsymbol{\sigma}_\mathbf{s} = K(J-1)\mathbf{I} + \frac{G}{J}\left(\mathbf{F}\mathbf{F}^\text{T} - J^{2/3}\mathbf{I}\right), \tag{4}$$

in which K and G are defined as

$$K = \frac{E}{3(1-2\nu)} \text{ and } G = \frac{E}{2(1+\nu)}, \tag{5}$$

in which E is Young's modulus and ν is Poisson's ratio (Wilson et al. 2005a).

The biphasic swelling model was implemented in a UMAT subroutine (Hsieh et al. 2005) and was validated by comparing the results for a 2D test case with Wilson et al.'s (2005a) results.

2.2 Geometry and boundary conditions

Incongruent contact surfaces were given physiological radii of the femur and tibia. The convex femoral indenter and concave tibial AC surface were 30 and 80 mm in radius, respectively (Peterson and Renström 2001). The tibial AC was 15 mm long in the radial direction and 2.1 mm thick (Ahmad et al. 2001). Four-node bilinear displacement-pore pressure elements (CAX4P) were used to discretise the model geometry (Figure 1).

In all models, the bottom surface of tibial cartilage was impermeable, and pore pressure on the upper surface was set at zero and thus free fluid flow was initially prescribed. As the tibial and the femoral surfaces came in contact, fluid flow normal to the contacting element surfaces was set to zero with FLOW and URDFIL subroutines (Warner et al. 2001; Keenan et al. 2009). Displacements of the nodes on the bottom plane were confined in all directions representing cartilage attachment to the subchondral bone tissue.

The creep response of the model was investigated by applying a ramp load of 30 N for 0.5 s, and then holding it constant until equilibrium was reached. We chose this load because it resulted in instantaneous axial deformations comparable with those measured *in vivo* (Liu et al. 2010). In addition, higher loading produced convergence difficulties in models that lacked integration.

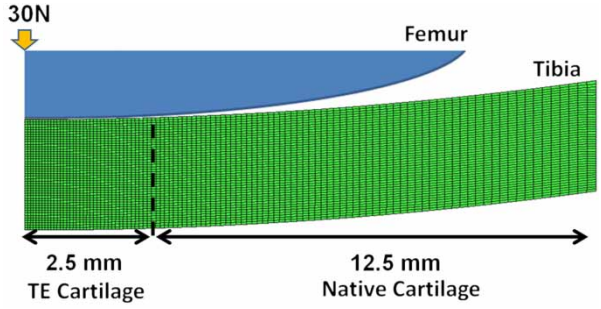

Figure 1. Schematic of the FE model for transplanted TE construct.

2.3 Material properties

AC material properties comparable to those found in the literature were assigned. The equivalent Young's modulus and Poisson's ratio for the solid matrix were set to 0.5 MPa and 0.15, respectively (Wilson et al. 2005a). It is well known that hydraulic permeability of AC is deformation dependent (Maroudas 1968; Lai and Mow 1980; Holmes and Mow 1990). Empirical exponential equations for deformation-dependent permeability of hydrogels and cartilage have been shown to be accurate over a wide range of permeabilities (Holmes and Mow 1990; Gu et al. 2003). van der Voet (1997) proposed a formulation of an exponential law for deformation-dependent permeability that can be implemented in Abaqus®:

$$k = k_0 \left(\frac{e+1}{e_0+1} \right)^M, \tag{6}$$

in which k_0 is the initial permeability, M is a positive constant, and e and e_0 are the current and initial void ratios (ratio of fluid volume fraction to solid volume fraction), respectively. We used the values proposed by Wilson et al. (2005b) for the constants: $M = 5$, $k_0 = 1.5 \times 10^{-15}$ m^4/Ns and $e_0 = 3$.

Although anisotropy and inhomogeneity of AC material properties are well documented (Huang et al. 2003; Wilson et al. 2007; Korhonen et al. 2008), they were not included in the model to simplify interpretation of the results. Initial FCD was set to 2×10^{-4} mmol/mm^3 (Mow et al. 1998; Wilson et al. 2005a). At the start of the simulation, the model was in equilibrium with a physiological salt solution of 1.5×10^{-4} mmol/mm^3. Geometric nonlinearity was accounted for by using NLGEOM option.

2.4 Cases studied

Full thickness chondral defects repaired with a TEC were modelled at the centre of the joint. The transplanted TEC was 5 mm in diameter (Figure 1). In some cases, the engineered tissue was assumed to have 15% reduced PG content and 65% lower initial modulus than native AC, whereas in other cases the mechanical properties were identical to the native tissue. Lower initial modulus and PG content values are in the range of properties previously reported (Cheng et al. 2009; Huang et al. 2009). To examine the effect of different TE construct properties and integration with native AC on the mechanical response of the joint, we investigated four different cases: (1) TEC with identical PG content and modulus to AC and fully integrated with native tissue (i.e. intact joint); equally stiff – integrated or ES-I, (2) TEC with 15% lower PG content and 65% lower modulus than AC and fully integrated with native tissue; less stiff – integrated or LS-I, (3) TEC with identical PG content and modulus to AC but no integration with native tissue; equally stiff – not integrated or ES-NI and (4) TEC with lower PG content and modulus than AC and no integration with native tissue; less stiff – not integrated or LS-NI (Table 1).

Full integration in ES-I and LS-I was represented by modelling transplant and native AC as a continuous geometry. In ES-NI and LS-NI cases, in which the TE construct and native AC were not integrated, the two tissues were modelled as separate geometries, and frictionless contact between the two was defined. Pore pressure continuity between cartilage on opposite sides of the interface was maintained. Integrated and not-integrated models consisted of 8400 and 18,900 CAX4P elements and 8591 and 19,292 nodes, respectively. In a preliminary study, the results were not significantly affected with further mesh refinement.

Table 1. TEC construct properties in different cases.

	Property		
Case	Initial modulus (MPa)	Initial FCD (mmol/mm^3)	Integration at the interface
Equally stiff – integrated (ES-I)	0.50	2.0×10^{-4}	Yes
Less stiff – integrated (LS-I)	0.17	1.7×10^{-4}	Yes
Equally stiff – not integrated (ES-NI)	0.50	2.0×10^{-4}	No
Less stiff – not integrated (LS-NI)	0.17	1.7×10^{-4}	No

3. Results

First our implementation of Wilson et al.'s (2005a) biphasic swelling model in ABAQUS was validated using a 2D test case. Results identical to original authors' were obtained in our simulations (data not shown).

The maximum axial deformation of the surface node at the centre of contact immediately after indentation was 13% of the total cartilage thickness for the intact joint (ES-I) and increased to 14, 15 and 16% in LS-I, ES-NI and LS-NI cases, respectively. All instantaneous maximum axial deformations lie in the range of *in-vivo* cartilage deformations reported by Liu et al. (2010) for the stance phase of gait. At equilibrium, the value of maximum axial deformation at the centre of contact for the intact joint (ES-I) was 25% of the total cartilage thickness and increased to 27, 27 and 29% in LS-I, ES-NI and LS-NI cases, respectively, at the same location.

The distribution pattern of contact stress at the cartilage surface was altered by changes in TEC material properties. The intact joint (ES-I) showed a peak contact stress at the centre of the indenter that decreased in the radial direction. Lack of integration and a mismatch in material properties of TEC/native cartilage both resulted in a contact stress concentration in native cartilage in the vicinity of defect rim (Figure 2). This contact stress concentration was accompanied by a decrease in contact stress in the adjacent region of TEC. Instantaneous contact stress at the centre of the indenter was ~ 0.57 MPa for both equal stiffness cases (ES cases). This contact stress was decreased by 26 and 23% for LS-I and LS-NI cases. The contact stress concentration at the rim of defect in cases LS-I, ES-NI and LS-NI resulted in, respectively 13, 13 and 25% higher contact stress than the intact joint (ES-I). This was accompanied by 12, 22 and 23% decrease in contact stress, respectively, in adjacent region of TEC compared with intact joint (Figure 2(a)). The alterations in contact stress with an implant that had inferior mechanical properties or a lack of integration persisted during the creep simulation. Equilibrium contact stress at the centre of the indenter was ~ 0.41 MPa for both ES cases (Figure 2(b)). This contact stress was decreased by approximately 50% for LS-I and LS-NI cases. Contact stress concentration in native cartilage at the rim of the defect in cases LS-I, ES-NI and LS-NI resulted in, respectively 15, 11 and 22% higher contact stress than an intact joint. At the same time, there was a 45, 36 and 59% decrease in contact stress, respectively, in adjacent region of TEC compared with intact joint (Figure 2(b)).

Load partitioning between the fluid phase and solid matrix was also investigated with our model. The contribution of pore pressure, swelling pressure and solid matrix stress to total normal stress for the surface node at the centre of contact was calculated

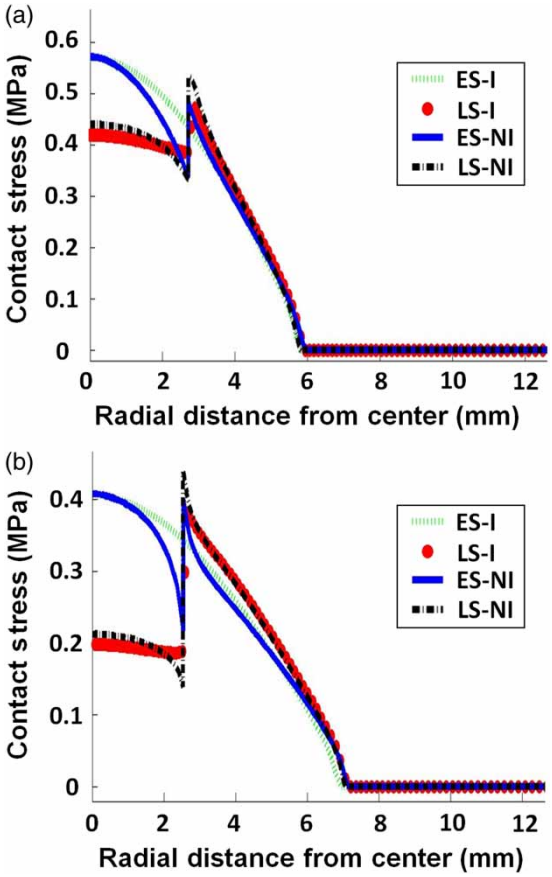

Figure 2. Contact stress at the articular surface, (a) instantaneous response and (b) equilibrium response.

(Figure 3(a),(b)). As expected for the instantaneous response, most of the load was supported by the fluid phase, as it supported 76–78% of the total load in implants with identical properties to native cartilage and 88% in less stiff implants. The PG swelling pressure supported nearly 8% of the total load in implants with stiffness equal to native cartilage, and 3–4% in implants with inferior properties. The magnitude of solid matrix stress was 94, 33, 84 and 35 kPa for ES-I, LS-I, ES-NI and LS-NI cases, respectively. The integration of the implant with the surrounding tissue did not have a large effect on load partitioning (Figure 3(a)).

At equilibrium, interstitial fluid pressurisation no longer supports the load, and normal stress is counteracted by swelling pressure and solid matrix stress. Compared with ES-I and ES-NI cases, total normal stress was reduced to roughly half in LS-I and LS-NI cases. The solid matrix supported 66, 48, 63 and 49% of the total normal stress for ES-I, LS-I, ES-NI and LS-NI cases, respectively. The remainder of total normal stress was supported by PG swelling pressure in all cases (Figure 3(b)).

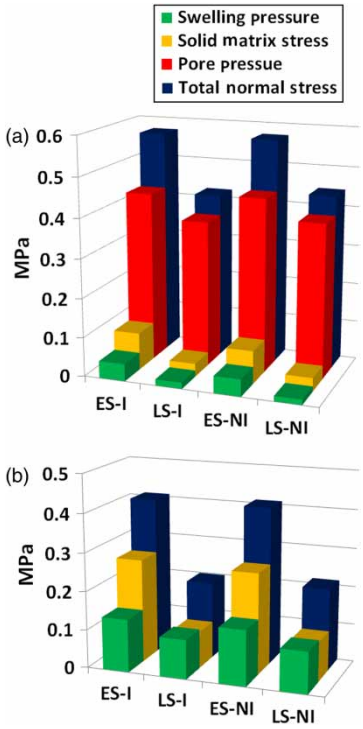

Figure 3. Partitioning of load for surface node at the centre of contact, (a) instantaneous response and (b) equilibrium response.

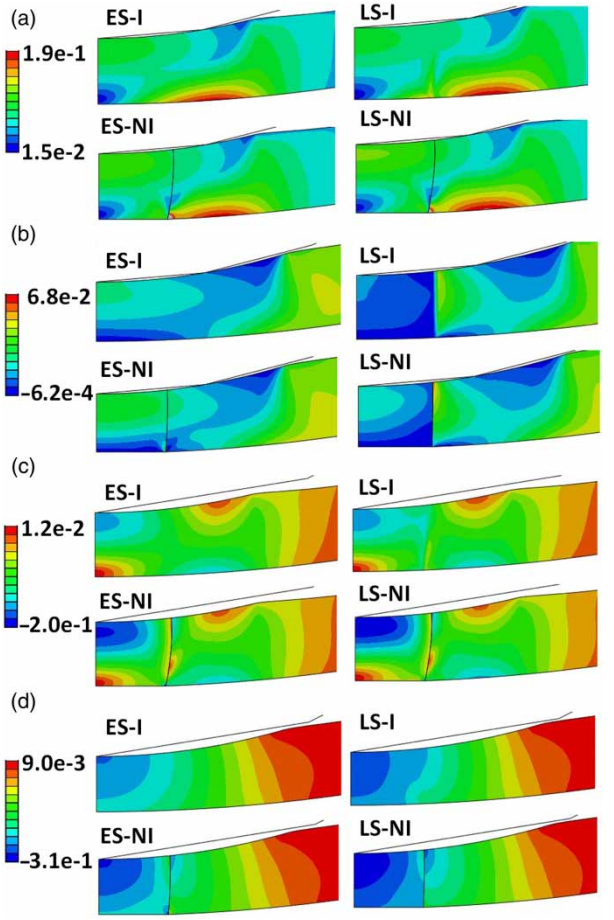

Figure 4. Maximum principal strain distribution, (a) instantaneous response and (b) equilibrium response. Minimum principal strain distribution, (c) instantaneous response and (d) equilibrium response.

Lack of integration and a mismatch in material properties only slightly alter the maximum (tensile) instantaneous principal strain at the boundary between TEC and native AC (Figure 4(a)). The highest instantaneous maximum principal strain occurs away from axis of symmetry at the native cartilage–bone interface for all analyses (Figure 4(a)). At equilibrium, in cases LS-I and LS-NI, the maximum principal strain in TEC in the vicinity of the interface near the surface decreased, whereas the maximum principal strain in adjacent native AC increased compared with an intact joint (Figure 4(b)).

The highest magnitude of minimum (compressive) principal strain was located near articular surfaces on the axis of symmetry in all cases and increased due to lack of integration and mismatch in mechanical properties (Figure 4(c)). Immediately after loading, the value of highest magnitude compressive principal strain on the axis of symmetry for the intact joint (ES-I) was -15% and increased to -16, -19 and -20% in LS-I, ES-NI and LS-NI cases, respectively (Figure 4(c)). The magnitude of the minimum (compressive) principal strain at equilibrium was the highest at the surface on the axis of symmetry for all cases. At equilibrium, the value of highest magnitude compressive principal strain at the surface on the axis of symmetry for intact joint (ES-I) was -27%, and increased to -29, -29 and -31% in LS-I, ES-NI and LS-NI cases, respectively, at the same location (Figure 4(d)).

Fluid velocity was also affected by TEC transplantation (Figure 5). In cases in which the TEC is not integrated to surrounding native AC (ES-NI and LS-NI), the relative fluid velocity shows a more non-uniform distribution at the TEC and native AC interface. This is likely due to high compression in both tissues at the contact interface.

The relative tangential motion (sliding) between TEC and native AC in NI cases was minimally affected by changes in TEC stiffness immediately after loading (Figure 6). Maximum instantaneous sliding between TEC/native AC was $\sim 118\,\mu m$ and was located at three-fourth of the cartilage depth. The location of the maximum relative sliding between TEC and native AC was nearly identical in the instantaneous and equilibrium response, thus results at equilibrium are not shown. A slight gap opening, orders of magnitude smaller than the relative

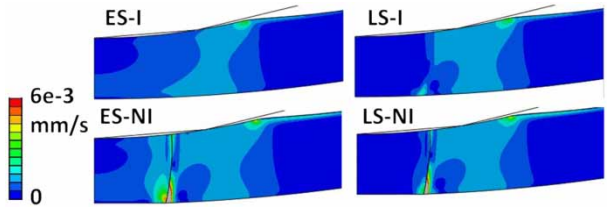

Figure 5. Relative fluid velocity distribution, instantaneous response.

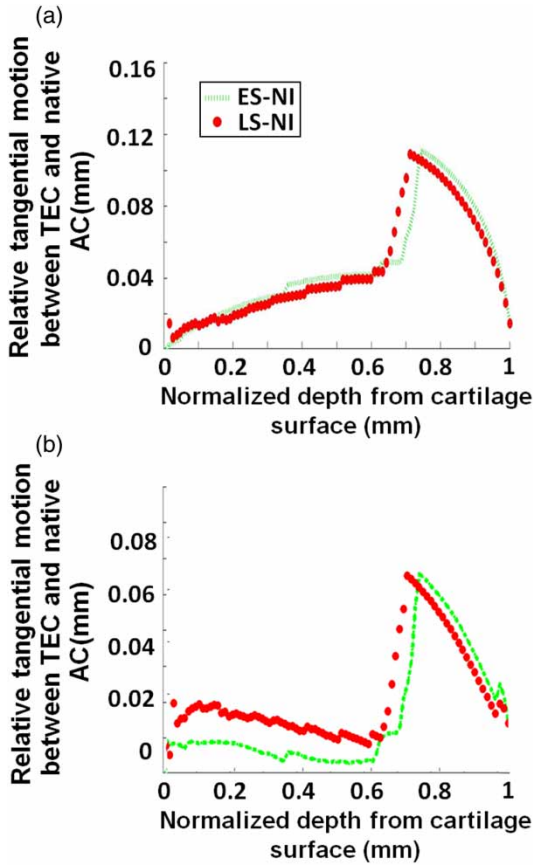

Figure 6. Relative tangential motion (sliding) between TEC and native AC, instantaneous response.

tangential sliding, was observed at two nodes at the surface, and the two tissue surfaces were in contact elsewhere (data not shown).

Instantaneous contact stress distribution at the interface between TEC and native AC was also minimally affected by the reduction in modulus and PG content of TEC (Figure 7(a)). The maximum instantaneous contact stress was located near cartilage–bone interface. At equilibrium, the contact stress was almost uniform across the interface and was ~20% lower in LS-NI than ES-NI case (Figure 7(b)).

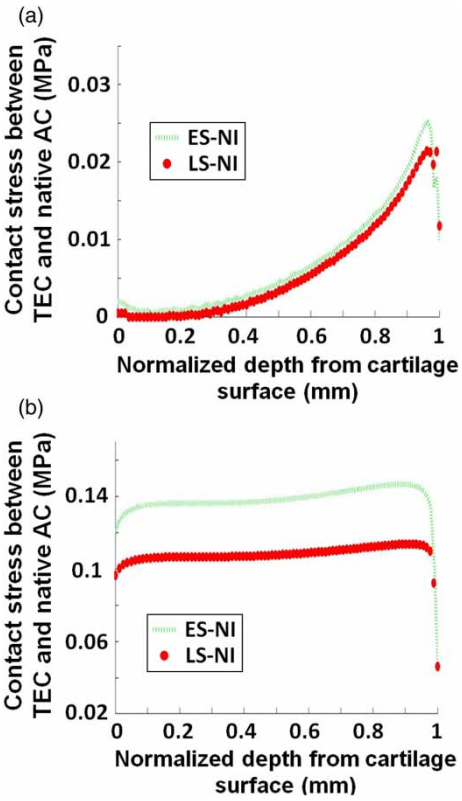

Figure 7. Contact stress distribution at the TEC/native AC interface, (a) instantaneous response, (b) equilibrium response.

4. Discussion

Tissue engineering offers great potential for the repair of chondral and osteochondral defects. Much effort has been put into engineering cartilage tissue that mimics native tissue (Butler et al. 2009). In spite of these efforts, it has proven to be very difficult to achieve TEC with chemical composition and mechanical properties that match those of native AC (Hunziker 2002; Zhang et al. 2009). Most tissue-engineered cartilage constructs have inferior mechanical properties to native AC, which not only affects mechanotransduction signals received by transplanted cells, but may also alter the mechanical environment of adjacent AC (Braman et al. 2005; Strauss et al. 2005) or in the worst case scenario the global response of the joint. To investigate these issues, FE models of engineered chondral tissue in the human tibiofemoral joint, including geometric and material property discontinuities at the interface between engineered and native cartilage, were created.

Our results for contact stress distribution at the articular surface (Figure 2) are consistent with experimental results, showing a contact stress concentration of 10–30% at the defect rim in full-thickness osteochondral defects of dog knees (Brown et al. 1991). Depending on the magnitude of loading, compressive and shear stress resulting from contact can induce either a catabolic or anabolic cellular response in chondrocytes located at or

near the surface of AC (Grodzinsky et al. 2000). In one study, chondrocyte apoptosis and matrix degradation in cartilage explants increased with peak stress in a dose-dependent manner (Loening et al. 2000). Our study, therefore, suggests that the observed excessive loading due to contact stress concentrations at the defect rim could result in a cellular response and may be detrimental to the structural integrity of the tissues.

Load partitioning between different phases plays an important role in the mechanical response of AC. The portion of the total load supported by the fluid phase at the articular surface of the intact joint in our model was 76%, which is very close to experimental results (Park et al. 2003). For the more compliant transplants, the fluid load support increased to 88% (Figure 3(a)). This increase in fluid load compensated for the lower stiffness of the matrix to some extent. Lower solid matrix stress due to increased load partitioning to the fluid phase can directly influence frictional properties of the articular surface due to biphasic lubrication (Krishnan et al. 2003, 2005; Ateshian 2009). It has been shown that the coefficient of friction increases linearly with increased load partitioning to solid matrix (Krishnan et al. 2004). On the basis of this criterion, our model suggests that TEC with inferior properties may exhibit a lower friction coefficient *in vivo* due to decreased solid matrix stress, all other factors being equal. On the other hand, the coefficient of friction of AC also depends on the contact stress. Increasing the contact stress from 0.2 to 0.5 MPa, while the percentage of fluid load support within the cartilage remained almost identical, decreased the coefficient of friction (Katta et al. 2007). However, further increase in the contact stress had the opposite effect and led to a higher coefficient of friction (Katta et al. 2008). On the basis of current experimental data, it is difficult to say which one of these effects will dominate the frictional response of TEC in our model.

Lower stiffness and lack of integration of the engineered tissue both lead to an increased magnitude in the minimum (compressive) principal strains in TEC. The largest magnitude of compressive principal strain in TEC was observed when both of these effects were combined (Figure 4(c),(d)). Guilak et al. (1995) subjected AC explants to physiological levels of matrix deformation and observed 19% local strain in the surface zone, which is close to local strains obtained in our study. According to their results, this local strain will decrease cellular height by 26% and cellular volume by 22%. It is known that cellular deformation is accompanied by deformations at the subcellular level in organelles such as the nucleus, rough endoplasmic reticulum and mitochondria (Szafranski et al. 2004). Lack of integration and lower stiffness of TEC increased the local compressive strains below the articular surface by 33% compared with intact joint in our study (Figure 4(b)). Thus our results suggest that the inferior properties of the TEC and lack of integration could lead to altered deformations at cellular and subcellular levels and significant changes in biosynthetic activity of the implanted cells.

It was observed that lack of integration introduces a slight strain discontinuity at the transplant/AC boundary (Figure 4(a)). The transplant with inferior properties introduced a discontinuity in the strain distribution, even when it was fully integrated with native AC (Figure 4(a)–(c)). Differences in strain magnitudes due to the discontinuity in strain distribution could cause perturbations in mechanical stimulus and affect the biological response of implanted cells and native chondrocytes.

Lack of integration resulted in higher compaction of both tissues, which in turn drove the fluid away from the interface (Figure 5). During normal activities, fluid flow in AC is mainly restricted to the superficial and transitional zones (Wong and Carter 2003). Compaction of TEC due to lack of integration induced higher fluid velocities in the middle and deep zones of TEC in ES-NI case, which does not occur in the intact joint. Fluid flow is implicated in changing pericellular concentration of macromolecular cytokines, growth factors, degradative enzymes, endogenous enzyme inhibitors, newly synthesised matrix molecules and nutrients (Grodzinsky et al. 2000). In addition, aggrecan synthesis has been linked to the spatial profile of fluid velocity in cartilage explants and TECs (Kim et al. 1994; Buschmann et al. 1999; Mauck et al. 2007). Thus alterations in fluid flow velocity and pattern observed in our study could alter the cellular response of both native chondrocytes and transplanted cells.

Integration of TEC to native cartilage plays a critical role and remains a major challenge in the long-term repair of chondral and osteochondral defects. As biomechanical characterisation of repair tissue at the site of integration *in vivo* is difficult, explants cultures of cartilage have been primarily used to study the integrative repair process (Reindel et al. 1995; Obradovic et al. 2001; DiMicco et al. 2002; Moretti et al. 2005; Gratz et al. 2006). It has been postulated that at early stages of the integrative repair process, molecular bridges span the interface between TEC and native AC (Ahsan and Sah 1999). Relative displacement between the engineered and native AC could interfere with initiation of integration and formation of molecular bridges. To investigate the effect of implant material properties on the integrative repair response, relative sliding at the implant/AC boundary was plotted. The relative sliding between surfaces was highly non-uniform (Figure 6). Decreased stiffness of the TEC did not change the magnitude of relative tangential motion between the TEC and native AC and only slightly changed the location of its maximum. Given our modelling assumptions, it can be suggested that an implant with inferior properties may not disrupt the integrative repair process anymore than an ideal implant. Although our results are dependent on the location of defect and loading

conditions, they show that models which resemble *in-vivo* loading conditions are needed to better characterise and understand complex displacements and loading that either integration tissue or adhesive layer is subjected to at the interface. FE techniques used for analysis of adhesively bonded joints such as cohesive elements could be beneficial to characterise biomechanical properties of repair tissue or adhesives (i.e. fibrin glue, tissue transglutaminase, photochemical welding) at the site of integration.

Similar to the results for relative sliding, contact stress was also plotted for the interface between TEC and native tissue. The contact stress distribution at the interface was non-uniform for the instantaneous response and uniform for the equilibrium response (Figure 7(a),(b)). The magnitude of contact stress was generally higher when the TEC had properties identical to those of native AC, suggesting that the tissues may be more likely to integrate in this case. Our results also show that near the articular surface, the contact stress is reduced to zero. However, little to no separation of the two tissues was observed at the interface (data not shown).

A number of simplifications in modelling the knee joint were made. To avoid problems associated with poroelastic contact between more than two deformable bodies, the femur was modelled as a rigid impermeable indenter. Modelling the opposing cartilage layer as a deformable material would give a more accurate representation of the mechanics in the knee. Owen and Wayne (2011) showed that loading with a deformable cartilage layer results in increased contact area and decreased axial deformation and pore pressure compared with a rigid impermeable indenter; thus our results overestimate the axial deformation and pore pressure. However, the same study also demonstrated that radial and axial stresses and strains are similar in models of repair cartilage with a rigid impermeable indenter or with a deformable cartilage layer. Furthermore, Owen and Wayne's (2011) results suggest that the rigid impermeable indenter may allow for reasonable comparisons between models in some instances. For example, the pore pressure is the highest in their 'NORMBOT' and lowest in their 'REP' models, regardless of how the indenter is modelled.

The menisci, which support approximately 50% of the load in the knee joint, were not modelled in the current study. A more detailed model should also include tendons, ligaments and muscle forces. Another simplification with regard to modelling tibial cartilage was that tension–compression nonlinearity was not included in the constitutive model. It is well known that collagen fibres contribute to higher tensile stiffness of AC and several computational models have successfully incorporated collagen fibres (Soulhat et al. 1999; Wilson et al. 2005b; Shirazi et al. 2008; Ateshian et al. 2009; Li et al. 2009; Shirazi and Shirazi-Adl 2009; Owen and Wayne 2011). Although arcade-shaped and depth-dependent collagen fibre distribution is a characteristic of native AC, TEC normally lacks organised collagen fibre distribution and is sufficiently modelled as isotropic. As our study was qualitative rather than quantitative in nature, and also to simplify interpretation of results, collagen fibres were not included in this study. This simplification of isotropic and homogenous material properties for both TEC and AC allowed us to observe, for example, that the location of the maximum relative tangential sliding, which occurs at ~70% of the tissue depth, appears to be inherent to the geometric conditions of the model. A more detailed constitutive model of AC should include depth-dependent inhomogeneity (i.e. water content, PG content, collagen content permeability), anisotropy, tension–compression nonlinearity and intrinsic viscoelasticity of the tissue (Soltz and Ateshian 2000; Huang et al. 2003; Wilson et al. 2007; Korhonen et al. 2008; Owen and Wayne 2011). Modelling anisotropy and the depth dependence of cartilage components could be helpful in designing TECs for the repair of focal chondral defects; it may be possible to optimise the depth-dependent properties of TECs to increase their load-bearing capacity and integration to the native tissue.

As AC in the knee is subjected to a wide variety of static and dynamic loading conditions (Grodzinsky et al. 2000), it will be useful to study the effect of more complex loading conditions and cyclic loading on transplanted TEC in future FE studies. Although axisymmetric models such as the ones presented here are not able to capture non-uniformities in contact stress distribution around the defect rim like 3D models do (Pena et al. 2007), they allow for other complexities such as a biphasic material representation, which is not normally included in 3D cartilage studies. In conclusion, both the material properties of TEC and integration to the surrounding cartilage alter the mechanical environment of both the engineered implant and the native tissue, and may negatively impact the phenotypic stability of the cells and the structural integrity of the tissues. The present simulations when combined with knowledge of molecular and cellular level behaviour of AC may be helpful in future designs and evaluations of osteochondral TE strategies and implantation techniques.

References

Ahmad CS, Cohen ZA, Levine WN, Ateshian GA, Mow VC. 2001. Biomechanical and topographic considerations for autologous osteochondral grafting in the knee. Am J Sports Med. 29:201–206.

Ahsan T, Sah RL. 1999. Biomechanics of integrative cartilage repair. Osteoarthr Cartilage. 7:29–40, doi:10.1053/joca.1998.0160

Ateshian GA. 2009. The role of interstitial fluid pressurization in articular cartilage lubrication. J Biomech. 42:1163–1176, doi:10.1016/j.jbiomech.2009.04.040

Ateshian GA, Rajan V, Chahine NO, Canal CE, Hung CT. 2009. Modeling the matrix of articular cartilage using a continuous fiber angular distribution predicts many observed phenomena. J Biomech Eng. 131:061003, doi:10.1115/1.3118773

Babalola OM, Bonassar LJ. 2009. Parametric finite element analysis of physical stimuli resulting from mechanical stimulation of tissue engineered cartilage. J Biomech Eng. 131:061014, doi:10.1115/1.3128672

Braman JP, Bruckner JD, Clark JM, Norman AG, Chansky HA. 2005. Articular cartilage adjacent to experimental defects is subject to atypical strains. Clin Orthop Relat Res. 430: 202–207.

Brown TD, Pope DF, Hale JE, Buckwalter JA, Brand RA. 1991. Effects of osteochondral defect size on cartilage contact stress. J Orthop Res. 9:559–567, doi:10.1002/jor.1100090412

Buschmann MD, Kim YJ, Wong M, Frank E, Hunziker EB, Grodzinsky AJ. 1999. Stimulation of aggrecan synthesis in cartilage explants by cyclic loading is localized to regions of high interstitial fluid flow. Arch Biochem Biophys. 366:1–7.

Butler DL, Goldstein SA, Guldberg RE, Guo XE, Kamm R, Laurencin CT, McIntire LV, Mow VC, Nerem RM, Sah RL, et al. 2009. The impact of biomechanics in tissue engineering and regenerative medicine. Tissue Eng Part B Rev. 15:477–484, doi:10.1089/ten.TEB.2009.0340

Cheng NC, Estes BT, Awad HA, Guilak F. 2009. Chondrogenic differentiation of adipose-derived adult stem cells by a porous scaffold derived from native articular cartilage extracellular matrix. Tissue Eng Part A. 15:231–241, doi:10.1089/ten.tea.2008.0253

Cicuttini F, Ding C, Wluka A, Davis S, Ebeling PR, Jones G. 2005. Association of cartilage defects with loss of knee cartilage in healthy, middle-age adults: a prospective study. Arthritis Rheum. 52:2033–2039, doi:10.1002/art.21148

DiMicco MA, Waters SN, Akeson WH, Sah RL. 2002. Integrative articular cartilage repair: dependence on developmental stage and collagen metabolism. Osteoarthr Cartilage. 10:218–225, doi:10.1053/joca.2001.0502

Ding C, Garnero P, Cicuttini F, Scott F, Cooley H, Jones G. 2005. Knee cartilage defects: association with early radiographic osteoarthritis, decreased cartilage volume, increased joint surface area and type II collagen breakdown. Osteoarthr Cartilage. 13:198–205, doi:10.1016/j.joca.2004.11.007

Duda GN, Maldonado ZM, Klein P, Heller MO, Burns J, Bail H. 2005. On the influence of mechanical conditions in osteochondral defect healing. J Biomech. 38:843–851, doi:10.1016/j.jbiomech.2004.04.034

Gratz KR, Wong VW, Chen AC, Fortier LA, Nixon AJ, Sah RL. 2006. Biomechanical assessment of tissue retrieved after *in vivo* cartilage defect repair: tensile modulus of repair tissue and integration with host cartilage. J Biomech. 39:138–146, doi:10.1016/j.jbiomech.2004.10.016

Grodzinsky AJ, Levenston ME, Jin M, Frank EH. 2000. Cartilage tissue remodeling in response to mechanical forces. Annu Rev Biomed Eng. 2:691–713, doi:10.1146/annurev.bioeng.2.1.691

Gu WY, Yao H, Huang CY, Cheung HS. 2003. New insight into deformation-dependent hydraulic permeability of gels and cartilage, and dynamic behavior of agarose gels in confined compression. J Biomech. 36:593–598.

Guilak F, Ratcliffe A, Mow VC. 1995. Chondrocyte deformation and local tissue strain in articular cartilage: a confocal microscopy study. J Orthop Res. 13:410–421, doi:10.1002/jor.1100130315

Hale JE, Rudert MJ, Brown TD. 1993. Indentation assessment of biphasic mechanical property deficits in size-dependent osteochondral defect repair. J Biomech. 26:1319–1325.

Holmes MH, Mow VC. 1990. The nonlinear characteristics of soft gels and hydrated connective tissues in ultrafiltration. J Biomech. 23:1145–1156.

Hsieh AH, Wagner DR, Cheng LY, Lotz JC. 2005. Dependence of mechanical behavior of the murine tail disc on regional material properties: a parametric finite element study. J Biomech Eng. 127:1158–1167.

Huang AH, Farrell MJ, Mauck RL. 2010. Mechanics and mechanobiology of mesenchymal stem cell-based engineered cartilage. J Biomech. 43:128–136, doi:10.1016/j.jbiomech.2009.09.018

Huang CY, Soltz MA, Kopacz M, Mow VC, Ateshian GA. 2003. Experimental verification of the roles of intrinsic matrix viscoelasticity and tension–compression nonlinearity in the biphasic response of cartilage. J Biomech Eng. 125:84–93.

Huang AH, Stein A, Tuan RS, Mauck RL. 2009. Transient exposure to transforming growth factor beta 3 improves the mechanical properties of mesenchymal stem cell-laden cartilage constructs in a density-dependent manner. Tissue Eng Part A. 15:3461–3472, doi:10.1089/ten.TEA.2009.0198

Hunziker EB. 2002. Articular cartilage repair: basic science and clinical progress. A review of the current status and prospects. Osteoarthr Cartilage. 10:432–463, doi:10.1053/joca.2002.0801

Huyghe J. 1997. Quadriphasic mechanics of swelling incompressible porous media. Int J Eng Sci. 35:793–802, doi:10.1016/S0020-7225(96)00119-X

Katta J, Jin ZM, Ingham E, Fisher J. 2008. Biotribology of articular cartilage – a review of the recent advances. Med Eng Phys. 30:1349–1363.

Katta J, Pawaskar SS, Jin ZM, Ingham E, Fisher J. 2007. Effect of load variation on the friction properties of articular cartilage. Proc Inst Mech Eng Part J. 221:175–181, doi:10.1243/13506501JET240

Keenan KE, Kourtis LC, Besier TF, Lindsey DP, Gold GE, Delp SL, Beaupré GS. 2009. New resource for the computation of cartilage biphasic material properties with the interpolant response surface method. Comput Meth Biomech Biomed Eng. 12:415–422.

Kelly DJ, Prendergast PJ. 2006. Prediction of the optimal mechanical properties for a scaffold used in osteochondral defect repair. Tissue Eng. 12:2509–2519, doi:10.1089/ten.2006.12.2509

Kim YJ, Sah RL, Grodzinsky AJ, Plaas AH, Sandy JD. 1994. Mechanical regulation of cartilage biosynthetic behavior: physical stimuli. Arch Biochem Biophys. 311:1–12, doi:10.1006/abbi.1994.1201

Korhonen RK, Julkunen P, Wilson W, Herzog W. 2008. Importance of collagen orientation and depth-dependent fixed charge densities of cartilage on mechanical behavior of chondrocytes. J Biomech Eng. 130:021003, doi:10.1115/1.2898725

Krishnan R, Kopacz M, Ateshian GA. 2004. Experimental verification of the role of interstitial fluid pressurization in cartilage lubrication. J Orthop Res. 22:565–570, doi:10.1016/j.orthres.2003.07.002

Krishnan R, Mariner EN, Ateshian GA. 2005. Effect of dynamic loading on the frictional response of bovine articular cartilage. J Biomech. 38:1665–1673, doi:10.1016/j.jbiomech.2004.07.025

Krishnan R, Park S, Eckstein F, Ateshian GA. 2003. Inhomogeneous cartilage properties enhance superficial

interstitial fluid support and frictional properties, but do not provide a homogeneous state of stress. J Biomech Eng. 125: 569–577.

Lai WM, Hou JS, Mow VC. 1991. A triphasic theory for the swelling and deformation behaviors of articular cartilage. J Biomech Eng. 113:245–258.

Lai WM, Mow VC. 1980. Drag-induced compression of articular cartilage during a permeation experiment. Biorheology. 17: 111–123.

Lattermann C, Kang RW, Cole BJ. 2006. What's new in the treatment of focal chondral defects of the knee? Orthopedics. 29:898–903.

Li LP, Cheung JT, Herzog W. 2009. Three-dimensional fibril-reinforced finite element model of articular cartilage. Med Biol Eng Comput. 47:607–615, doi:10.1007/s11517-009-0469-5

Liu F, Kozanek M, Hosseini A, Van de Velde SK, Gill TJ, Rubash HE, Li G. 2010. *In vivo* tibiofemoral cartilage deformation during the stance phase of gait. J Biomech. 43:658–665, doi:10.1016/j.jbiomech.2009.10.028

Loening AM, James IE, Levenston ME, Badger AM, Frank EH, Kurz B, Nuttall ME, Hung HH, Blake SM, Grodzinsky AJ, et al. 2000. Injurious mechanical compression of bovine articular cartilage induces chondrocyte apoptosis. Arch Biochem Biophys. 381:205–212, doi:10.1006/abbi.2000.1988

Maroudas A. 1968. Physicochemical properties of cartilage in the light of ion exchange theory. Biophys J. 8:575–595, doi:10.1016/S0006-3495(68)86509-9

Mauck RL, Byers BA, Yuan X, Tuan RS. 2007. Regulation of cartilaginous ECM gene transcription by chondrocytes and MSCs in 3D culture in response to dynamic loading. Biomech Model Mechanobiol. 6(1–2):113–125, doi:10.1007/s10237-006-0042-1

McNickle AG, Provencher MT, Cole BJ. 2008. Overview of existing cartilage repair technology. Sports Med Arthrosc. 16:196–201, doi:10.1097/JSA.0b013e31818cdb82

Minas T, Nehrer S. 1997. Current concepts in the treatment of articular cartilage defects. Orthopedics. 20:525–538.

Mononen ME, Julkunen P, Toyras J, Jurvelin JS, Kiviranta I, Korhonen RK. 2010. Alterations in structure and properties of collagen network of osteoarthritic and repaired cartilage modify knee joint stresses. Biomech Model Mechanobiol. 10:357–369, doi:10.1007/s10237-010-0239-1

Moretti M, Wendt D, Schaefer D, Jakob M, Hunziker EB, Heberer M, Martin I. 2005. Structural characterization and reliable biomechanical assessment of integrative cartilage repair. J Biomech. 38:1846–1854, doi:10.1016/j.jbiomech.2004.08.021

Mow VC, Atheshian GA, Lai WM, Gu WY. 1998. Effects of fixed charges on the stress–relaxation behavior of hydrated soft tissues ina confined compression problem. Int J Solids Struct. (35):4945–4962.

Obradovic B, Martin I, Padera RF, Treppo S, Freed LE, Vunjak-Novakovic G. 2001. Integration of engineered cartilage. J Orthop Res. 19:1089–1097, doi:(10.1016/S0736-026601)00030-4

Owen JR, Wayne JS. 2006. Influence of a superficial tangential zone over repairing cartilage defects: implications for tissue engineering. Biomech Model Mechanobiol. 5:102–110, doi:10.1007/s10237-006-0022-5

Owen JR, Wayne JS. 2011. Contact models of repaired articular surfaces: influence of loading conditions and the superficial tangential zone. Biomech Model Mechanobiol, doi:10.1007/s10237-010-0247-1

Park S, Krishnan R, Nicoll SB, Ateshian GA. 2003. Cartilage interstitial fluid load support in unconfined compression. J Biomech. 36:1785–1796.

Pena E, Calvo B, Martinez MA, Doblare M. 2007. Effect of the size and location of osteochondral defects in degenerative arthritis. A finite element simulation. Comput Biol Med. 37:376–387, doi:10.1016/j.compbiomed.2006.04.004

Peterson L, Renström P. 2001. Sports injuries: their prevention and treatment. 3rd ed. London: Martin Dunitz.

Reindel ES, Ayroso AM, Chen AC, Chun DM, Schinagl RM, Sah RL. 1995. Integrative repair of articular cartilage *in vitro*: adhesive strength of the interface region. J Orthop Res. 13: 751–760, doi:10.1002/jor.1100130515

Richter W. 2007. Cell-based cartilage repair: illusion or solution for osteoarthritis. Curr Opin Rheumatol. 19:451–456, doi:10.1097/BOR.0b013e3282a95e4c

Sellards RA, Nho SJ, Cole BJ. 2002. Chondral injuries. Curr Opin Rheumatol. 14:134–141.

Shirazi R, Shirazi-Adl A. 2009. Computational biomechanics of articular cartilage of human knee joint: effect of osteochondral defects. J Biomech. 42:2458–2465, doi:10.1016/j.jbiomech.2009.07.022

Shirazi R, Shirazi-Adl A, Hurtig M. 2008. Role of cartilage collagen fibrils networks in knee joint biomechanics under compression. J Biomech. 41:3340–3348, doi:10.1016/j.jbiomech.2008.09.033

Smith CL, Mansour JM. 2000. Indentation of an osteochondral repair: sensitivity to experimental variables and boundary conditions. J Biomech. 33:1507–1511.

Soltz MA, Ateshian GA. 2000. A conewiselinearelasticity mixture model for the analysis of tension–compression nonlinearity in articular cartilage. J Biomech Eng. 122:576, doi:10.1115/1.1324669

Soulhat J, Buschmann MD, Shirazi-Adl A. 1999. A fibril-network-reinforced biphasic model of cartilage in unconfined compression. J Biomech Eng. 121:340–347.

Strauss EJ, Goodrich LR, Chen CT, Hidaka C, Nixon AJ. 2005. Biochemical and biomechanical properties of lesion and adjacent articular cartilage after chondral defect repair in an equine model. Am J Sports Med. 33:1647–1653, doi:10.1177/0363546505275487

Szafranski JD, Grodzinsky AJ, Burger E, Gaschen V, Hung HH, Hunziker EB. 2004. Chondrocyte mechanotransduction: effects of compression on deformation of intracellular organelles and relevance to cellular biosynthesis. Osteoarthr Cartilage. 12:937–946, doi:10.1016/j.joca.2004.08.004

van der Voet A. 1997. A comparison of finite element codes for the solution of biphasic poroelastic problems. Proc Inst Mech Eng H. 211:209–211.

van Loon R, Huyghe JM, Wijlaars MW, Baaijens FPT. 2003. 3D FE implementation of an incompressible quadriphasic mixture model. Int J Numer Methods Eng. 57:1243–1258, doi:10.1002/nme.723

Warner MD, Taylor WR, Clift SE. 2001. A method for determining contact between a non-porous surface and articular cartilage in a biphasic FE model. In: Middleton J, Shrive NG, Pande GN, editors. Computer methods in biomechanics and biomedical engineering – 3. Lisbon: Gordon and Breach Science Publishers. p. 207–212.

Wayne JS, Woo SL, Kwan MK. 1991a. Application of the u–p finite element method to the study of articular cartilage. J Biomech Eng. 113:397–403.

Wayne JS, Woo SL, Kwan MK. 1991b. Finite element analyses of repaired articular surfaces. Proc Inst Mech Eng H. 205: 155–162.

Wilson W, Huyghe JM, van Donkelaar CC. 2007. Depth-dependent compressive equilibrium properties of articular cartilage explained by its composition. Biomech Model Mechanobiol. 6:43–53, doi:10.1007/s10237-006-0044-z

Wilson W, van Donkelaar CC, Huyghe JM. 2005a. A comparison between mechano-electrochemical and biphasic swelling theories for soft hydrated tissues. J Biomech Eng. 127: 158–165.

Wilson W, van Donkelaar CC, van Rietbergen B, Huiskes R. 2005b. A fibril-reinforced poroviscoelastic swelling model for articular cartilage. J Biomech. 38:1195–1204, doi:10.1016/j.jbiomech.2004.07.003

Wong M, Carter DR. 2003. Articular cartilage functional histomorphology and mechanobiology: a research perspective. Bone. 33:1–13.

Wu JZ, Herzog W, Hasler EM. 2002. Inadequate placement of osteochondral plugs may induce abnormal stress–strain distributions in articular cartilage – finite element simulations. Med Eng Phys. 24:85–97.

Zhang L, Hu J, Athanasiou KA. 2009. The role of tissue engineering in articular cartilage repair and regeneration. Crit Rev Biomed Eng. 37:1–57.